J Solid State Electrochem (2011) 15:2571–2579
DOI 10.1007/s10008-010-1235-1

ORIGINAL PAPER

Intermediate temperature ionic conductivity of $Sm_{1.92}Ca_{0.08}Ti_2O_{7-\delta}$ pyrochlore

Karinh E. J. Eurenius · Henrik Karnøe Bentzer · Nikolaos Bonanos · Elisabet Ahlberg · Christopher S. Knee

Received: 11 May 2010 / Revised: 3 November 2010 / Accepted: 4 November 2010 / Published online: 25 November 2010
© Springer-Verlag 2010

Abstract The results of concentration cell electromotive force methods (EMF) and electrochemical impedance spectroscopy measurements on the pyrochlore system $Sm_{1.92}Ca_{0.08}Ti_2O_{7-\delta}$ are presented. The data have been used to estimate total and partial conductivities and determine transport numbers for protons and oxide ions under various conditions. The EMF techniques employed include corrections for electrode polarisation resistance. The measurements were performed using wet and dry atmospheres in a wide p_{O_2} range using mixtures of H_2, N_2, O_2, and H_2O in the temperature region where proton conductivity was expected (500–300 °C). The impedance measurements revealed the conductivity to be mainly ionic under all conditions, with the highest total conductivity measured being 0.045 S/m under wet oxygen at 500 °C. Both bulk and grain boundary conductivity was predominantly ionic, but electronic conductivity appeared to play a slightly larger part in the grain boundaries. EMF data confirmed the conductivity to be mainly ionic, with oxide ions being the major conducting species at 500 °C and protons becoming increasingly important below this temperature.

Keywords Proton conductor · Pyrochlore · $Sm_2Ti_2O_7$ · Concentration cell electromotive force method (EMF) · Electrochemical impedance spectroscopy (EIS) · Transport numbers

K. E. J. Eurenius · E. Ahlberg · C. S. Knee
Department of Chemistry, University of Gothenburg,
SE-412 96, Gothenburg, Sweden

H. K. Bentzer (✉) · N. Bonanos
Fuel Cells and Solid State Chemistry Division,
Risø National Laboratory for Sustainable Energy,
Technical University of Denmark,
PO Box 49, DK-4000, Roskilde, Denmark
e-mail: henrik.bentzer@risoe.dk

Present Address:
K. E. J. Eurenius
Department of Materials Engineering, School of Engineering,
University of Tokyo,
7-3-1 Hongo, Bunkyo-ku,
Tokyo 113-8656, Japan

Introduction

Proton-conducting perovskite systems have been extensively examined as electrolyte materials [1–5]. Proton-conducting pyrochlores of general formula $A_2B_2O_7$ can be compared with perovskite-based compounds and may also be considered as potential candidates for electrolytes in solid-oxide fuel cells. Acceptor-doped pyrochlores generally exhibit an increase in the ionic conductivity compared with undoped system, with oxide ion charge carriers dominant at high temperature [6, 7], whilst significant proton conductivity can emerge at lower temperatures in hydrated gases [8, 9]. Studies of pyrochlores typically show proton conductivities of about one to two orders of magnitude lower than the best-performing perovskites in the intermediate temperature range (200–700 °C) [10]. Finding new electrolyte materials with adequate conductivity in this temperature interval would be beneficial from a technological point of view in particular with respect to reducing the operating temperature of fuel cells. Therefore, gaining a better understanding of the proton conductivity in pyrochlore systems and finding ways to increase it is of interest.

Studies have recently been presented on proton conductivity in acceptor-doped pyrochlore materials [11, 12]. $Er_{1.96}Ca_{0.04}Ti_2O_{7-\delta}$[11] was found to exhibit high levels

of proton mobility in the grain boundaries but the bulk conductivity showed no dependence on the presence of water vapour. Recently, a detailed study on the proton conduction in $Sm_{1.92}Ca_{0.08}Ti_2O_{7-\delta}$ and $Sm_2Ti_{1.92}Y_{0.08}O_{7-\delta}$ was published [12]. Characterisation by infrared spectroscopy and thermogravimetric analysis (TGA) were used to detect the presence of dissolved protons in the materials. An increase of the bulk conductivity was observed for both samples below 500 °C for wet conditions and measurements in O_2/D_2O and Ar/D_2O revealed an isotopic dependence, indicating that the increased conductivity is due to proton conduction. The A-site-doped sample, $Sm_{1.92}Ca_{0.08}Ti_2O_{7-\delta}$, displayed both a higher proton concentration and conductivity compared with the B-site-doped phase, and was therefore chosen for the more detailed investigations of the conduction species presented herein.

In this work electrochemical impedance spectroscopy (EIS) was carried out on $Sm_{1.92}Ca_{0.08}Ti_2O_{7-\delta}$ to determine the conductivity as a function of p_{O_2} in dry and wet atmospheres and at various temperatures. The results have been compared with the previously presented data from a single atmosphere supplied cell [12]. Furthermore, electromotive force (EMF) measurements combined with active load corrections [13], were carried out to determine the transport numbers associated with the conduction processes.

Theory

Defect chemistry

To understand the underlying processes giving rise to the conductivity, a defect chemical model is formulated. The concentration of the conducting species (i), denoted c_i, is directly related to its conductivity (σ_i) through its mobility (μ_i,) and charge (z_i):

$$\sigma_i = z_i e c_i \mu_i \tag{1}$$

Even if the mobility of the conducting species is not known, the p_{O_2} dependency of the conductivity will still reveal what the dominant point defects in the system are, as long as the mobility can be assumed not to be a function of oxygen partial pressure.

Kröger–Vink notation is used for all point defects. In this model, all oxygen sites will be treated as equal. Protonic defects are described as hydroxide ions on oxygen sites. This is believed to be an accurate description of the defect itself, with proton transport occurring via the Grotthuss mechanism [14].

In acceptor doped pyrochlores, the dopants are assumed to be primarily charge compensated by oxygen vacancies over a wide temperature and oxygen partial pressure range. These can also be formed according to the reaction in Eq. 2:

$$\begin{aligned} &O_O{}^X \rightleftharpoons 1/2O_{2(g)} + V_O{}^{\bullet\bullet} + 2e' \\ &K_O = p_{O_2}{}^{1/2}[V_O{}^{\bullet\bullet}]n^2 \end{aligned} \tag{2}$$

The internal electronic equilibrium is described by Eq. 3, where the K_e is the internal electronic equilibrium constant:

$$\begin{aligned} &\text{nil} \rightleftharpoons e' + h^{\bullet} \\ &K_e = \text{np} \end{aligned} \tag{3}$$

In hydrogen-containing atmospheres, protonic defects can be created according to Eq. 4:

$$\begin{aligned} &2O_O{}^X + H_{2(g)} \rightleftharpoons 2OH_O{}^{\bullet} + 2e' \\ &K_{H_2} = [OH_O{}^{\bullet}]^2 p_{H_2}^{-1} n^2 \end{aligned} \tag{4}$$

Protonic defects can also be introduced through interaction with water as shown in Eq. 5:

$$\begin{aligned} &V_O{}^{\bullet\bullet} + O_O{}^X + H_2O_{(g)} \rightleftharpoons 2OH_O{}^{\bullet} \\ &K_{H_2O} = [OH_O{}^{\bullet}]^2 p_{H_2O}^{-1} [V_O{}^{\bullet\bullet}]^{-1} \end{aligned} \tag{5}$$

Equation 5 can also easily be found by subtracting Eq. 2 and adding the gaseous equilibrium between water, hydrogen and oxygen in Eq. 6 from Eq. 4.

$$H_2O_{(g)} \rightleftharpoons 1/2O_{2(g)} + H_{2(g)} \tag{6}$$

The complete electroneutrality equation for the system is:

$$\left[Ca_{Sm}'\right] + n = 2\left[V_O^{\bullet\bullet}\right] + p + \left[OH_O^{\bullet}\right] \tag{7}$$

To aid the analysis of the conductivity data, simplified electroneutrality conditions can be formulated, where only the dominant species are taken into account. The concentration of other species can then be calculated if the equilibrium constants are known, but their dependency on oxygen and water vapour pressure can be found directly from the equations.

If the dopant level is significant, the concentration of oxygen vacancies will be dominated by the dopant level. In dry conditions, the concentration of oxygen vacancies is dominant and protonic defects negligible, and a simplified electroneutrality condition can be written:

$$\left[Ca_{Sm}'\right] = 2\left[V_O^{\bullet\bullet}\right] \tag{8}$$

The oxide ionic conductivity depends on the concentration of oxygen vacancies, and will therefore not vary with p_{O_2}, while the p_{O_2} dependency of the n- and p-type

electronic conductivity can be calculated from the oxygen vacancy creation reaction (Eq. 2):

$$\begin{array}{l} K_{\mathrm{O}} = p_{\mathrm{O_2}}^{1/2}[V_{\mathrm{O}}^{\bullet\bullet}]n^2 \\ \Updownarrow \\ n \propto p_{\mathrm{O_2}}^{-1/4} \\ \Updownarrow \\ p \propto p_{\mathrm{O_2}}^{1/4} \end{array} \tag{9}$$

At low $p_{\mathrm{O_2}}$ a situation may arise in which the material is sufficiently reduced that electrons take over as the species charge compensating the oxygen vacancies. The simplified charge neutrality condition then becomes:

$$n = 2\left[V_{\mathrm{O}}^{\bullet\bullet}\right] \tag{10}$$

The $p_{\mathrm{O_2}}$ dependence of electronic and oxide ionic conductivities can be expressed by Eq. 11:

$$\begin{array}{l} K_{\mathrm{O}} = p_{\mathrm{O_2}}^{1/2}[V_{\mathrm{O}}^{\bullet\bullet}]n^2 = \frac{1}{2}p_{\mathrm{O_2}}^{1/2}n^3 \\ \Updownarrow \\ n \propto p_{\mathrm{O_2}}^{-1/6} \\ \Updownarrow \\ p \propto p_{\mathrm{O_2}}^{1/6} \end{array} \tag{11}$$

Similarly, at high $p_{\mathrm{O_2}}$, the electron hole conductivity may rise up to a level where it becomes the charge compensator for the dopant, giving a simplified electroneutrality condition as stated by Eq. 12:

$$\left[\mathrm{Ca}_{\mathrm{Sm}}^{'}\right] = p \tag{12}$$

In this situation, the concentration of oxygen vacancies will decrease as $p_{\mathrm{O2}}{}^{-1/2}$.

When water vapour is introduced, protonic defects are created. Assuming the simplified electroneutrality condition in Eq. 8, the concentration of protonic defects relate to the partial pressure of water vapour as follows:

$$\begin{array}{l} K_{\mathrm{H_2O}} = [\mathrm{OH}_{\mathrm{O}}^{\bullet}]^2 p_{\mathrm{H_2O}}^{-1}[V_{\mathrm{O}}^{\bullet\bullet}]^{-1} \\ \Updownarrow \\ [\mathrm{OH}_{\mathrm{O}}^{\bullet}] \propto p_{\mathrm{H_2O}}^{1/2} \end{array} \tag{13}$$

As the concentration of protons increases, they can eventually overtake oxygen vacancies as the species charge compensating the dopant:

$$\left[\mathrm{Ca}_{\mathrm{Sm}}^{'}\right] = \left[\mathrm{OH}_{\mathrm{O}}^{\bullet}\right] \tag{14}$$

which leads to the following water vapour partial pressure dependencies for the other conducting species:

$$\begin{array}{l} [V_{\mathrm{O}}^{\bullet\bullet}] \propto p_{\mathrm{H_2O}}^{-1} \\ n \propto p_{\mathrm{H_2O}}^{1/2} \\ p \propto p_{\mathrm{H_2O}}^{-1/2} \end{array} \tag{15}$$

It should be noted that at the moderate temperatures and oxygen partial pressures employed in this work, the material is expected to remain in the extrinsic ionic conductive region.

The concentration cell EMF method

The EMF method is based on an open cell voltage measurement on a sample equipped with two reversible electrodes and subjected to a gradient in chemical potential. If small gradients are used, an average transport number can be assumed. The voltage measured over the sample will then be equal to:

$$E_{\mathrm{EMF}} = -\frac{RT}{nF} t_{\mathrm{i}} \ln \frac{p_2}{p_1} \tag{16}$$

where R, T, n and F are the universal gas constant, the temperature, the number of electrons transferred and Faraday's number, t_i is the average transport number and p_2 and p_1 are the partial pressures of the active species on either side of the sample. Comparing this to the theoretical voltage calculated using the Nernst Eq. 17:

$$E_{\mathrm{Nemst}} = -\frac{RT}{nF} \ln \frac{p_2}{p_1} \tag{17}$$

it is clear that the average transport number can be calculated by simply dividing the measured voltage with the calculated voltage (Eq. 18):

$$t_{\mathrm{i}} = \frac{E_{\mathrm{EMF}}}{E_{\mathrm{Nemst}}} \tag{18}$$

For systems where both oxide ion and proton conductivity are expected, the equilibrium between hydrogen, oxygen and water vapour must be taken into account. The total voltage developed over the sample can be calculated from partial pressures of gaseous species and transport numbers of oxide ions and protons (t_{O} and t_{p}) according to Eqs. 19 and 20:

$$E_{\mathrm{EMF}} = \frac{RT}{4F}(t_{\mathrm{O}} + t_{\mathrm{H}}) \ln \frac{p_{\mathrm{O_2}}^2}{p_{\mathrm{O_2}}^1} - \frac{RT}{2F}(t_{\mathrm{H}}) \ln \frac{p_{\mathrm{H_2O}}^2}{p_{\mathrm{H_2O}}^1} \tag{19}$$

or

$$E_{\mathrm{EMF}} = \frac{RT}{2F}(t_{\mathrm{O}}) \ln \frac{p_{\mathrm{H_2O}}^2}{p_{\mathrm{H_2O}}^1} - \frac{RT}{2F}(t_{\mathrm{O}} + t_{\mathrm{H}}) \ln \frac{p_{\mathrm{H_2}}^2}{p_{\mathrm{H_2}}^1} \tag{20}$$

Using these two equations as guidelines, it is possible to set up concentration cell measurements to determine the total ionic transport number, or the transport number of only oxide ions or protons. Keeping the gas phase equilibrium between oxygen, hydrogen and water vapour in mind, the experiment can be set up to create a gradient over the sample in only one species, as described elsewhere [15].

Correction methods

When using the EMF method, electrode polarisation resistance can possibly lead to underestimation of ionic

transport numbers. Two methods for correcting for high electrode polarisation resistance are reported in the literature; one based entirely on impedance measurements [16], and one based on impedance coupled with a variable load measurement [13]. The high polarisation resistances expected in this work would require time consuming impedance measurements down to very low frequencies, or alternatively extrapolations down to low frequency regions which would introduce a large uncertainty. Therefore, the second method, where only relatively high frequency impedance measurements are required, originally developed by Gorelov [13], was chosen.

The current driven by a Nernstian voltage E_{Nernst} in a sample with ionic, electronic and electrode polarisation resistances R_{i}, R_{e} and R_{η} and electrode over potential η can be described as Eq. 21:

$$I = \frac{(E_{\mathrm{Nernst}} - \eta)}{(R_{\mathrm{i}} + R_{\mathrm{e}})} = \frac{E_{\mathrm{meas}}}{R_{\mathrm{e}}} \tag{21}$$

The overpotential is assumed to be in the linear regime, which is a reasonable assumption at low voltage perturbations. Expressing the potential that would be measured between the electrodes in terms of R_{e}, R_{i} and t_{i} gives:

$$E_{\mathrm{meas}} = \frac{t_{\mathrm{i}} E_{\mathrm{Nernst}}}{1 + \frac{R_{\eta}}{R_{\mathrm{i}}+R_{\mathrm{e}}}} \tag{22}$$

For systems with a small electrode polarisation resistance, this will reduce to the original Wagner expression (Eq. 16). When R_{η} is significant, failing to take the electrode polarisation into account and correcting for it will give an underestimation of t_{i}. In practice, this is done by connecting a variable resistor (R_{b}) in parallel to the sample. This will increase the electronic conductivity of the entire system by an amount ($1/R_{\mathrm{b}}$). An equivalent circuit describing such a setup is shown in Fig. 1. The relation between theoretical and measured voltages for this system can be written as:

$$\frac{E_{\mathrm{Nernst}}}{E_{\mathrm{meas}}} - 1 = (R_{\mathrm{i}} + R_{\eta})\left(\frac{1}{R_{\mathrm{e}}} + \frac{1}{R_{\mathrm{b}}}\right) \tag{23}$$

Here, the left hand side of the expression is proportional to the sample's electronic conductivity ($1/R_{\mathrm{e}}$). If R_{b} is varied, E_{meas} will change and plotting $E_{\mathrm{Nernst}}/E_{\mathrm{meas}}-1$ against $1/R_{\mathrm{b}}$ will yield a straight line with a slope of $(R_{\mathrm{i}}+R_{\eta})$.

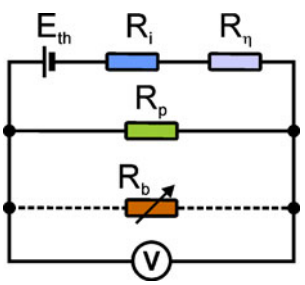

Fig. 1 Equivalent circuit of a concentration cell adapted from ref. [13]. See text for further details

Furthermore, the intercept at the y-axis give $(R_{\mathrm{i}}+R_{\eta})/R_{\mathrm{e}}$ and the extrapolated intersection at the x-axis give $-1/R_{\mathrm{e}}$. By performing an EIS measurement on the sample, the total bulk resistance, R_{T}, can be determined and the electronic transport number (t_{e}) can be expressed:

$$t_{\mathrm{e}} = \frac{R_{\mathrm{T}}}{R_{\mathrm{e}}} \tag{24}$$

Assuming only one ionic conduction path, the ionic transport number corrected for electrode polarisation resistance is:

$$t_{\mathrm{i}} = 1 - t_{\mathrm{e}} \tag{25}$$

As noted elsewhere [15], this correction method is not applicable if both protonic and oxide ionic conductivity is significant. Precise figures for transport numbers for both species are thus not always possible to obtain, but by using EIS and EMF data, a relatively good understanding of the material can be achieved.

Experimental

$Sm_{1.92}Ca_{0.08}Ti_2O_{7-\delta}$ was prepared via conventional solid state reactions of high purity reactants (Sm_2O_3 (99.9%), $CaCO_3$ (99.9%) and TiO_2 (99.9%)) as described in previous studies [16]. The powder was then ball-milled (150 rpm, 90 min) using zirconia balls after a fraction was taken aside to be used as sacrificial powder during sintering. The powders were mixed with a binder (polyvinyl alcohol 2% *w*/*w*) and pressed into pellets They were pressed uniaxially (73.5 MPa) and then as isostatically (325 MPa) in evacuated latex containers followed by sintering carried out in air (1650 °C, 100 h). The microstructure of the pellets was examined using a Zeiss SUPRA 35 scanning electron microscope (SEM).

The $Sm_{1.92}Ca_{0.08}Ti_2O_{7-\delta}$ pellet chosen for the EIS measurements was lightly polished, had a thickness of 2.08 mm and a relative density of 89%. The EIS was measured (4.5 MHz–1 Hz) with a Hioki 3532-50 LCR HiTESTER in a purpose built conductivity cell. The surface of the pellet was painted with Pt-paste (~0.55 cm^2) and the data were collected upon cooling (500–300 °C) in 50 °C interval steps (30–60 min equilibrium time) under a flow of gas (100–1% $O_2/O_2+H_2O/H_2+H_2O$ in N_2). The p_{O_2} was measured using a Nernst type cell built in house.

For the EMF setup, the $Sm_{1.92}Ca_{0.08}Ti_2O_{7-\delta}$ pellet (1.55 mm thick, density 86% of the theoretical value) was fitted with platinum electrodes and rigged inside an alumina tube (Fig. 2) in accordance with previous studies [15]. Gas to the inner and outer compartments was supplied through stainless steel tubes from a mixer setup. For wetting, the gas was bubbled through H_2O bottles in a fridge kept at

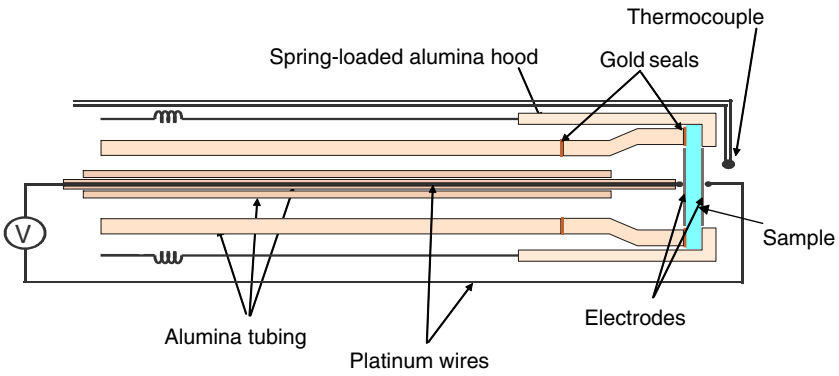

Fig. 2 Diagram of the measurement rig

12 °C, giving approximately 1% water vapour in the gas. Mixing the dry and wet gas enabled control of the water content of the gas. The water vapour concentration was measured using a Dewlux moisture meter from MCM Ltd, Wetherby UK, with analog output.

The experiments were carried out to find the transport numbers for oxide ions (t_O) and protons (t_H); the gas setup for the experiments is displayed in Table 1. The temperatures were decreased from 500 to 300 °C in steps of 100 °C with varying equilibration times (30 min – 2 h) depending on temperature and gas content. The Gorelov corrections for electrode irreversibility were performed at the maximum gas concentration gradient.

Results and discussion

The EIS data were fitted using ZSimpWin 3.21 from Echem Software. Voigt type equivalent circuits were used with a number of sub-circuits in series, each sub-circuit consisting of a resistor and a constant phase element in parallel. The inductance of the cell is known, and was corrected for, before fitting the data. Quasi equivalent capacitances were calculated for each individual RQ-couple. The highest frequency arc typically had a quasi equivalent capacitance in the order of 10^{-11} F cm^{-2}, while the next arc gave values around 10^{-9} F cm^{-2}. These values are typical for bulk and grain boundary conductivity respectively. A lower frequency arc is also observed. This arc, which is very dispersed in most of the measurements, represents the impedance related to various electrode processes. For some of the data, only the initial onset of the electrode arc was present in the data. In such cases, it was fitted with only a constant phase element without a resistor. The platinum electrodes did not cover the entire faces of the pellet, leading to fringing effects. Through final element modelling the error in conductivity was estimated to be approximately 12% and was corrected for.

In Fig. 3 the changes in conductivity with oxygen partial pressure are shown. In general only small changes are observed. Only at 500 °C is a clear increase of conductivity with increasing oxygen pressure observed at the high p_{O_2} end. The data obtained at 500 °C was fitted to Eq. 26:

$$\sigma_{tot} = \sigma_{ion} + \sigma_p^0 p_{O_2}^p + \sigma_n^0 p_{O_2}^{-n} \quad (26)$$

where the subscripts σ_{tot} is the total (measured) conductivity, σ_{ion} is the ionic conductivity, assumed independent of p_{O_2}, ${\sigma_p}^0$ and ${\sigma_n}^0$ are p- and n-type conductivity at $p_{O_2} = 1$, and p and n are positive fitted values to describe the p_{O_2} dependence of the two electronic conductivities. In the fit, both p and n come to a value of approximately 0.014, which is not consistent with any known defect chemical model. The small increase in conductivity that is observed at high and low p_{O_2} could merely be the onset of p- and n-type conductivity, and data from a wider range of oxygen

Table 1 Concentration cell setups

Experimental configuration	Gas in outer compartment (fixed)	Gas added in inner compartment	Transport number determined
A	100% O_2 (dry)	Dry N_2	t_O
B	O_2+H_2O (1%)	Dry O_2	t_H
C	6% H_2, 1% H_2O+N_2	Dry N_2	t_H
D	6% H_2, 1% H_2O+N_2	Dry 6% H_2 in N_2	t_O

The gas in the outer compartment was kept fixed while the gas in the inner compartment was varied to create a gradient by adding the gas noted in steps of 0%, 20%, 50%, 80% and 90%

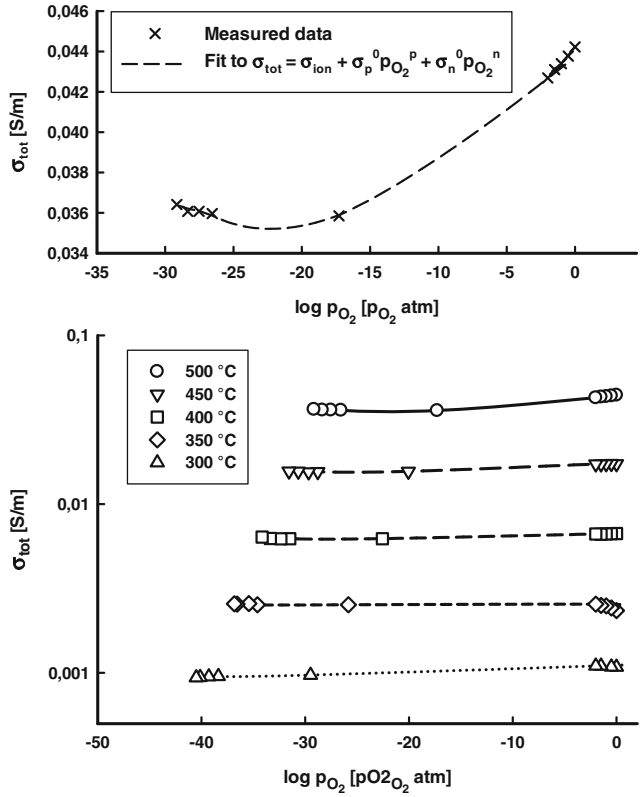

Fig. 3 Conductivity vs. log p_{O_2} at 500 °C (*top*) and conductivity at 500–300 °C vs. log p_{O_2} (*bottom*), all in 1% H_2O. The *lines joining the points in the bottom graph* are guides for the eye only

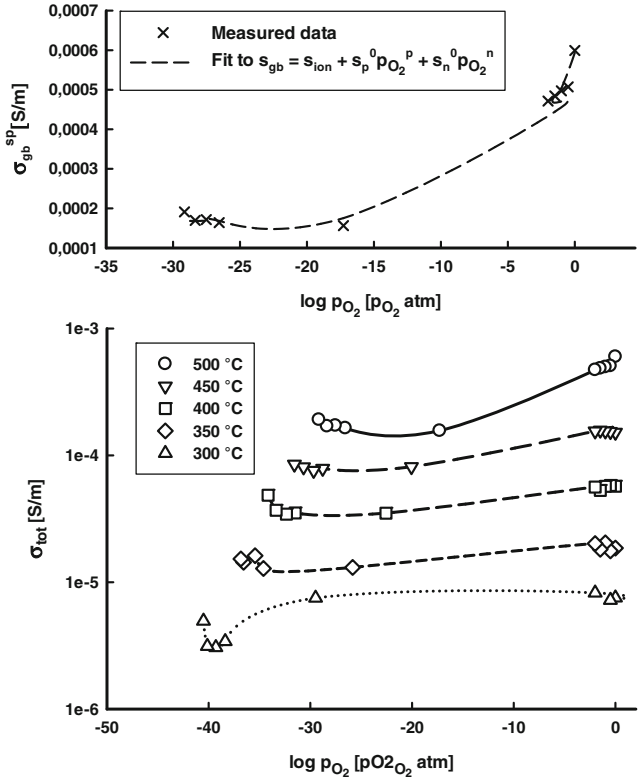

Fig. 4 Specific grain boundary conductivity vs. p_{O_2} at 500 °C (*top*) and specific grain boundary conductivity vs. log p_{O_2} at 300–500 °C (*bottom*), all in 1% H_2O. The *lines joining the points in the bottom graph* are guides for the eye only

partial pressures would be needed to extract their true p_{O_2} dependencies. At lower temperatures, the p_{O_2} dependency of the conductivity was even smaller, and no fitting was attempted.

A similar plot was constructed for the grain boundary conductivity of the material (Fig. 4), and it is immediately clear that a larger dependency on p_{O_2} is present both at high and low p_{O_2} over the entire temperature range. Again, a fit was made of the data from 500 °C, this time yielding *p*- and *n*-exponents of around 0.055. This is still far lower than predicted from the defect chemical model.

As expected the conductivity increases with temperatures and moisture content of the gas. When the temperature is increased, the difference in conductivity of wet and dry runs in oxygen becomes smaller, and at 500 °C they were close to identical. The same trend was observed in the previous measurements [12]. The data from 300 °C in this study gave similar values for the conductivity under dry conditions ($3.75\ 10^{-6}$ Scm^{-1}) as the previous study ($1.6{\cdot}10^{-6}$ Scm^{-1}) [12]. Under wet O_2 similar results are also obtained for the two studies ($1.2{\cdot}10^{-5}$ [12] vs. $1.75\ 10^{-5}$ S cm^{-1}). However, an increase in conductivity in dry argon compared with dry oxygen was reported, indicating n-type conductivity. A similar behaviour was not observed here, even when submitting the sample to atmospheres significantly more reducing than dry argon. The larger conductivity in dry Ar compared with dry O_2 found previously at low temperatures is most likely due to unintentional uptake of moisture during the measurements in Ar. The experimental setup was later modified to avoid this problem by introducing two silica drying tubes for the dry runs.

To examine whether some structural or compositional differences between the samples used in [12] and the samples used for the present work could account for the difference in conductivity vs. p_{O_2} behaviour between the two measurement series, both samples were investigated using scanning electron microscopy. Back scattered mode revealed a few, darker, grains dispersed in both samples. Energy dispersive X-ray spectroscopy indicated that these grains were very rich in calcium, while containing little titanium. Since this secondary phase is present in a too small amount to significantly influence the conductivity, and, furthermore, appeared to be present in roughly the same amount in both samples, it cannot explain the difference in conductivity vs. p_{O_2} behaviour between these measurements and those in [12]. It could, however, indicate that the calcium doping level is slightly above the actual solubility limit.

Dry measurements were not performed in hydrogen atmospheres to protect the sample from overly reducing conditions. The clear difference between wet and dry conductivity measurements can be seen in Fig. 5, which shows Arrhenius plots in wet O_2, dry O_2 and wet 6% H_2 in N_2. The two curves for wet gases are very similar, with the one obtained in oxygen being slightly higher at high temperatures, possibly due to the onset of *p*-type electronic conductivity. The marked difference between the dry and the wet runs, which increases with decreasing temperature, is ascribed to proton conductivity. This is in agreement with TGA data from a previous study on the material, which showed a mass loss beginning at around 375 °C and completing at around 500 °C [12].

As the present conductivity measurements were performed in the temperature range where the proton concentration changes, it was not possible to calculate a true activation energy for the proton conductivity. Measurements at a significantly higher water vapour partial pressure, so as to make sure that the material is saturated with protonic defects over a range of temperatures, would be required. The activation energy found for measurements performed in dry oxygen was 1.0 eV. This is comparable to the previously reported results of 0.93 eV in dry O_2 and 0.58 eV in H_2O and D_2O atmospheres [12].

Grain boundary conductivity has been shown for other systems to be limiting [17], but in this material they appear to only have a minor influence on the total conductivity. SEM analysis revealed a typical grain size of ~10 μm and using the brick layer model [18, 19] to illustrate the grain boundaries as described elsewhere [17], allowed a grain boundary thickness of approximately 5 nm to be estimated. In similar Sn-based pyrochlores [20] the calculated grain boundary thickness was almost ten times larger (~45 nm).

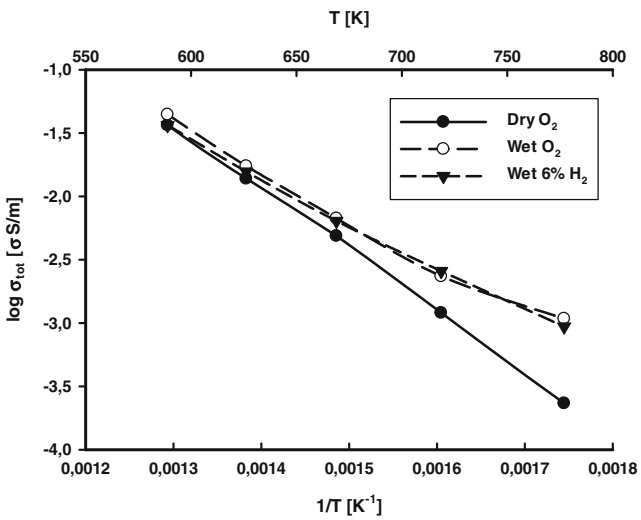

Fig. 5 Arrhenius plots of conductivity of $Sm_{1.92}Ca_{0.08}Ti_2O_{7-\delta}$ under dry and wet (1% H_2O) gas in 100% O_2 and 6% H_2 in N_2

From the grain size and grain boundary thickness the specific grain boundary conductivity can be calculated, and is shown to be about 100–400 times lower than the total conductivity. The p_{O_2} dependency of the grain boundary conductivity (Fig. 4) is stronger than that for bulk. The specific grain boundary conductivity decreases with decreasing oxygen partial pressure at constant temperature, while the bulk conductivity is overall constant. The fact that the p_{O_2} dependency of conductivity in the grain boundaries remains small, along with the fact that the it also increases when introducing water vapour in the atmosphere suggests that proton conduction also occurs in the grain boundaries but with a much lower conductivity than for the grain interior (bulk). For $Er_{1.96}Ca_{0.04}Ti_2O_{6.98}$ [11] proton conduction at the grain boundary was found to be significant but the bulk conductivity was dominated by oxide ion charge carriers. The reason for this differing behaviour may be linked to the subtleties of the synthesis routes. Fjeld et al. [11] report the presence of a Si impurity at the grain boundary originating possibly from the glass beaker used to prepare the initial solution of Er_2O_3 and $CaCO_3$.

The EMF measurements were carried out to find t_O and t_H. Investigations to determine the former were based on an oxygen concentration cell using dry oxygen and dry nitrogen/oxygen mixtures. t_H was evaluated at both high and low oxygen partial pressures. For a low p_{O_2} estimate of t_H, wet hydrogen diluted with nitrogen is used on one side of the sample, and the same gas mixed with dry inert gas (nitrogen) on the other side. In this manner, the hydrogen/water vapour ratio is kept constant and no unintentional oxygen partial pressure gradient is created. At high p_{O_2} a gradient in hydrogen partial pressure is created by using fixed levels of oxygen and water vapour on one side of the sample, while varying the oxygen/water vapour ratio, and thereby the hydrogen partial pressure, on the other side. Similarly, a gradient in oxygen can be made at low p_{O_2} by varying the water vapour partial pressure while maintaining a fixed hydrogen partial pressure on both sides. This measurement was also attempted, but only gave interpretable results at 500 °C. Given the results, it seems likely that this is due to the fact that proton conductivity is far higher than oxide ion conductivity, and even a slight unintended gradient in hydrogen partial pressure will obscure any EMF from the oxygen gradient.

The active load correction was carried out at the largest concentration gradient for each measurement series by adding a variable resistor to the circuit and recording the resulting change in EMF. Figure 6 shows the measured EMF data to determine t_H in oxidising conditions at 400 °C along with the data for the electrode polarisation resistance correction.

As expected, electrode polarisation resistance was significant in all measurements. In oxidising atmospheres,

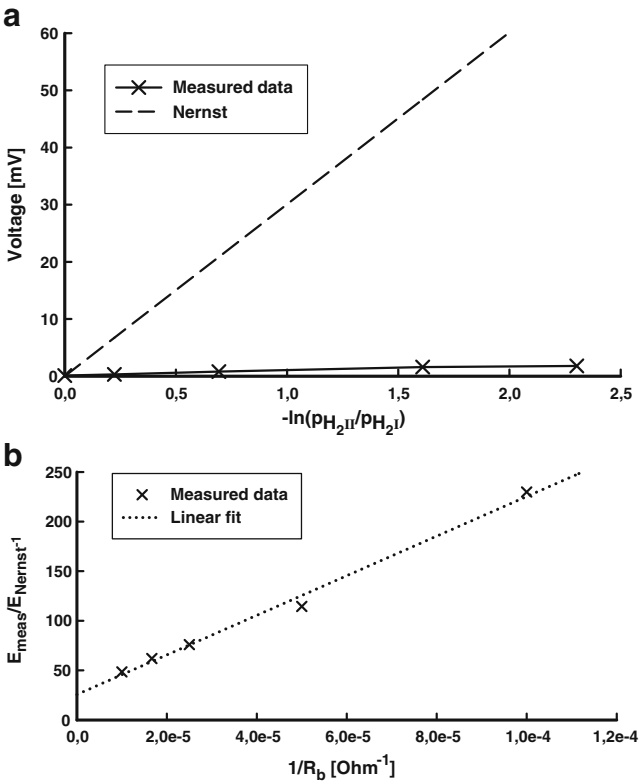

Fig. 6 Typical EMF measurement data from wet O_2 (t_H) 400 °C, configuration B in Table 1 (**a**), and active load measurement for electrode polarisation resistance correction of the same measurement (**b**)

impedance data showed it to be around a factor of 20 larger than the sample resistance at 500 °C and increasing with decreasing temperature. Electrode polarisation resistance was much lower in reducing atmospheres. At the lowest temperatures, this means that the entire electrode contribution to the impedance was not measured, but had to be extrapolated, since very low frequencies would have had to be employed to measure them. For the active load measurement, the resistor introduced in parallel needs to be of the same order of magnitude as the internal electronic resistance, i.e. the electronic resistance of the sample. Introducing a much smaller electronic resistance caused some drift in the EMF values. This explains for example the corrected proton transport number of 1.06 that was measured at high p_{O_2} at 300 °C. The uncorrected and corrected EMF data, along with the calculated transport numbers, are summarised in Table 2.

Despite the high electrode polarisation resistance, there is a clear trend in the data. At 300 and 400 °C in wet conditions the proton transport number is close to unity while the transport number for oxide ions is close to zero at these temperatures. At 500 °C the trend is reversed, with the oxide ionic transport number being close to unity and the protonic close to zero. This is in good agreement with previous results, where protons were shown to leave the compound as the temperature is increased towards 500 °C [12]. It is, however, not possible from these data to completely exclude the possibility that some protonic conductivity remains at 500 °C, or that some oxide ionic conductivity is still present at lower temperatures, since the necessary correction methods are not valid for systems with more than two conduction paths. It is also worth noting that the electrode polarisation resistance and the necessary correction for it is much greater in dry and oxidising conditions than in wet and reducing. This behaviour is in excellent agreement with the behaviour of platinum electrodes on ytterbium-doped strontium cerate [21].

Conclusions

The combined EIS and EMF measurements show that the conduction in $Sm_{1.92}Ca_{0.08}Ti_2O_{7-\delta}$ is mainly ionic. At 500 °C oxide ion transport dominates with a transport number, $t_O > 0.98$, while at 300 and 400 °C proton conduction takes over in wet conditions. Using the active load correction method, protons appear to be the majority charge carrier at both 300 and 400 °C, in both reducing and oxidising wet conditions. Using this correction method we were able to estimate reasonably reliable ionic transport numbers in the region where electrode polarisation resistance dominated. The partial pressure dependences suggested that electronic conduction probably plays

Table 2 Transport numbers for protons and oxide ions

		Configuration (see Table 1)		300 °C	400 °C	500 °C
t_O	High	A	Uncorrected	–	0	0.073
			Corrected	–	0	0.986
	Low	D	Uncorrected	–	–	0.75
			Corrected	–	–	0.991
t_H	High	B	Uncorrected	0.08	0.026	0
			Corrected	1.06	0.947	0
	Low	C	Uncorrected	0.42	0.34	0
			Corrected	0.876	0.924	0

a larger role in the grain boundaries than in the grain interior but the total conductivity is dominated by and practically equal to bulk conduction in this temperature interval.

Acknowledgements This work has been supported by the Swedish Research Council (Vetenskapsrådet) and by Risø-DTU as part of the project "Initiatives for Hydrogen Separation Membranes".

References

1. Iwahara H (1995) Solid State Ionics 77:289–298
2. Scherban T, Nowick AS (1989) Solid State Ionics 35:189–194
3. Bonanos N, Ellis B, Mahmood MN (1991) Solid State Ionics 44:305–311
4. Ahmed I, Eriksson SG, Ahlberg E, Knee CS, Berastegui P, Johansson LG, Rundlöf H, Karlsson M, Matic A, Börjesson L, Engberg D (2006) Solid State Ionics 177:1395–1403
5. Kreuer KD (2003) Annu Rev Mater Res 33:333–359
6. Yamamura H, Nishino H, Kakinuma K, Nomura K (2003) J Ceram Soc Jan 111:902–906
7. Kramer SA, Tuller HL (1995) Solid State Ionics 82:15–23
8. Omata T, Okuda K, Tsugimoto S, Otsuka-Yao-Matsuo S (1997) Solid State Ionics 104:249–258
9. Labrincha JA, Frade JR, Marques FMB (1997) Solid State Ionics 99:33–40
10. Omata T, Otsuka-Yao-Matsuo S (2001) J Electrochem Soc 148: E252–E261
11. Fjeld H, Haugsrud R, Gunnaes AE, Norby T (2008) Solid State Ionics 179:1849–1853
12. Eurenius KEJ, Ahlberg E, Ahmed I, Eriksson SG, Knee CS (2010) Solid State Ionics 181:148–153
13. Gorelov VP (1988) Elektrokhimiya 24:1380–1381
14. de Grotthuss CJT (1806) Ann Chim 58:54
15. Bentzer HK, Bonanos N, Phair JW (2010) Solid State Ionics 181:249–255
16. Liu M, Hu H (1996) J Electrochem Soc 143:L109–L112
17. Fleig J, Maier J (1998) J Electrochem Soc 145:2081–2089
18. van Dijk T, Burggraaf AJ (1981) Phys Status Solidi A 63:229–240
19. Verkerk MJ, Middelhuis BJ, Burggraaf AJ (1982) Solid State Ionics 6:159–170
20. Eurenius KEJ, Ahlberg E, Knee CS (2010) Solid State Ionics 181:1577–1585
21. Potter AR, Baker RT (2006) Solid State Ionics 177:1917–1924